A HIGH-RESOLUTION RAPIDLY-UPDATED METEOROLOGICAL DATA ANALYSIS SYSTEM FOR AVIATION APPLICATIONS

C. S. Lau *, J. T. K. Wan and M. C. Chu
Department of Physics, The Chinese University of Hong Kong, Hong Kong, China

P. W. Li
Hong Kong Observatory, Hong Kong, China

1. INTRODUCTION

A high spatial- and temporal-resolution meteorological data analysis system is under development for identifying and monitoring mesoscale to microscale weather phenomena over the Hong Kong International Airport (HKIA) and its vicinity. The system is adapted from NOAA Global Systems Division's Local Analysis and Prediction System (LAPS), which is a data assimilation system that can ingest most types of meteorological observation data efficiently compared with other data assimilation procedures such as 3DVAR and 4DVAR. The major advance of our system is the use of high-resolution, high-quality background and observation data in a small domain with a spatial resolution of 150 m, compared to a few kilometres in typical LAPS domains. This enables users to have a detailed study of disrupted wind flow over HKIA and its surroundings. This also helps users or forecasters to grip the whole picture of the atmosphere from the system at a glance, without looking at different observation data separately. This paper presents the design and the performance of the system.

2. DESIGN OF THE SYSTEM

The system is adapted from LAPS in the version of laps-0-29-11, which was released in July 2006. Several parts such as the ingestion of background data and radar data are amended. This will be discussed in the following sections.

2.1 *Domain*

The HKIA is situated over open water on an island connected to the Lantau Island, a hilly landmass with a top height of 934 m. The air flowing through the hills may bring windshear and turbulence to the airport. Thus the domain is designed to cover the whole Lantau Island, with HKIA located around the center of the domain. The area of the domain is about 30 km × 25 km, with a horizontal resolution of 150 m.

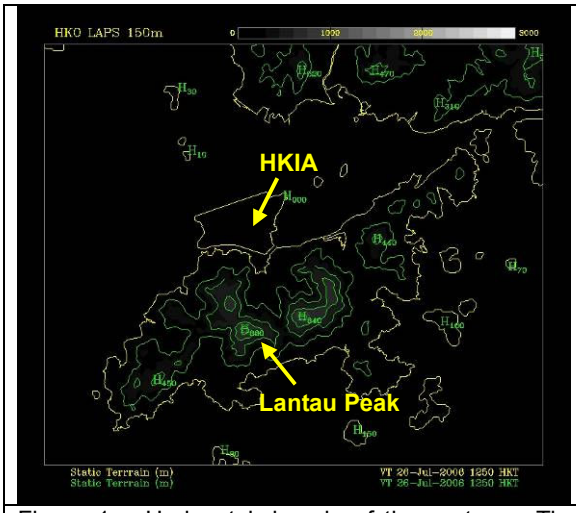

Figure 1 – Horizontal domain of the system. The central flat area is the HKIA, where its south is the Lantau Island.

In order to investigate the wind profile near the surface, the pressure intervals of the vertical domain are set at 5 or 10 hPa in levels below 900 hPa, and 50 hPa otherwise.

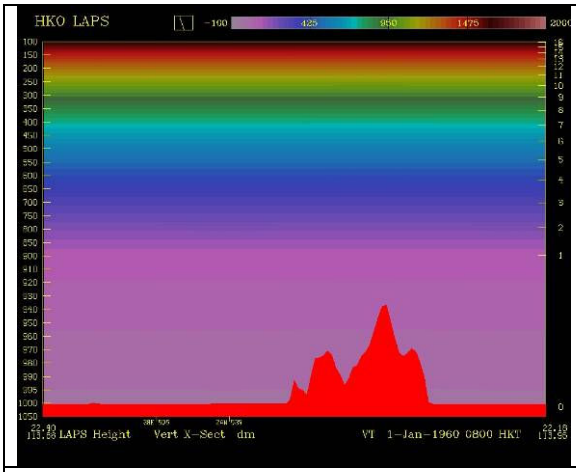

Figure 2 – Vertical domain of the system. The lower part of the figure shows the cross-section of Lantau Peak, the highest peak on the Lantau Island.

* *Corresponding author address*: Chi-Shing Lau, Department of Physics, The Chinese University of Hong Kong, Shatin, Hong Kong, China; e-mail: harrycslau@gmail.com.

High quality geographical data, including 3" terrain data and 3" land-use data, are remapped to the 150 m domain grids. This helps improve the wind field analysis in more details.

2.2 *Background field*

Observations are fitted to the background field using Barnes analysis and successive correction scheme to generate the analysis fields during the wind analysis. As our system is designed for a very small domain, a high-resolution background field is adopted (Fig. 3b).

(a)

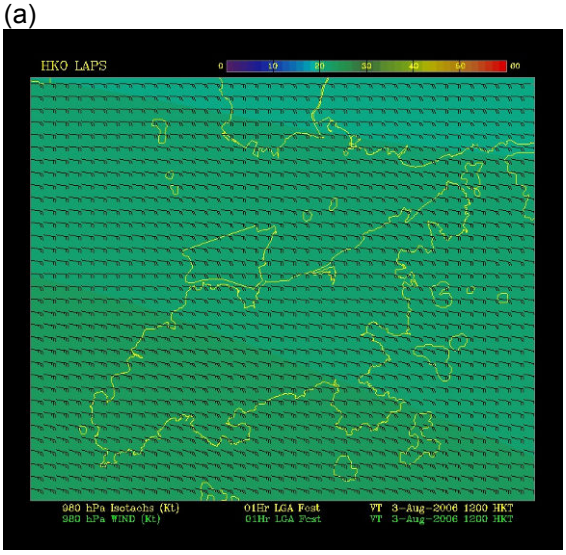

(b)

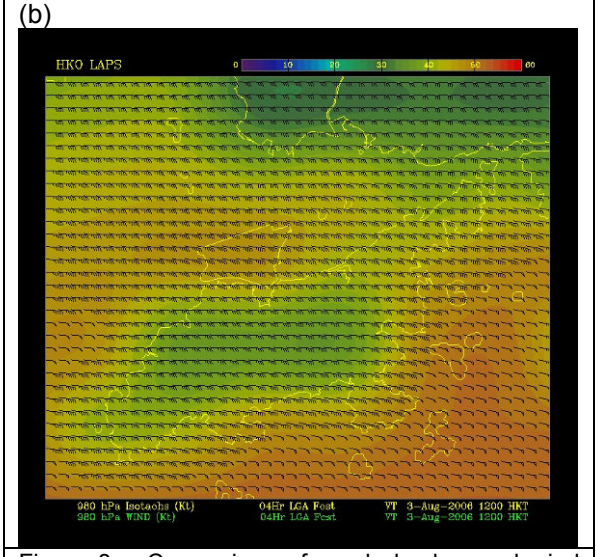

Figure 3 – Comparison of purely background wind field in 3 August 2006, where (a) from a 20-km mesh model, and (b) from 5-km mesh NHM. It can be seen that data in 5-km mesh is much more detailed.

The 5-km mesh data from the non-hydrostatic model (NHM) originally developed by JMA is chosen as the background field. The advantages of the NHM data include: (i) its horizontal resolution is sufficiently high for our purposes, and (ii) the data is updated every 1 hour.

2.3 *Observation Data*

Various observation data are ingested into the system. There are 21 automatic weather stations, weather buoys and anemometers, updated every 1 minute, to provide surface observations,. In addition, the FY-2C satellite visible and infrared digital data, updated hourly, are ingested to provide cloud information. Hourly data from aircrafts, radiosonde and two wind profilers are ingested.

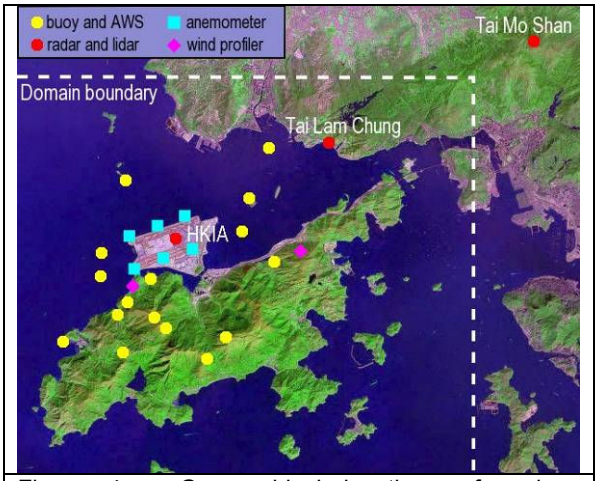

Figure 4 – Geographical locations of various meteorological observation instruments.

Besides the conventional data, additional remote sensing data from two weather radars, including a long-range S-band Doppler weather radar, a Terminal Doppler Weather Radar (TDWR), and wind data from a Doppler LIDAR are also ingested into the system. Figure 4 shows the geographical locations of the above observational platforms.

The long-range weather radar is situated in Tai Mo Shan (TMS), the highest peak in Hong Kong. It has 12 PPI scans with elevations from 0.0 to 34.0 degrees. The gate spacing of each scan is 250 m with a maximum range of 300 km. The data are updated every 6 minutes. It mainly provides the wind and reflectivity data for middle and upper levels of the atmosphere.

The TDWR is situated at Tai Lam Chung, facing the HKIA. It has 30 PPI scans with elevations from 0.6 to 39.6 degrees. The gate spacing of each scan is 150 m with a maximum range of 90 km. The TDWR data are available every minute in hazardous mode, and every 6

minutes under normal situation. It mainly provides the wind and reflectivity data for lower levels of the atmosphere under rainy situations.

The LIDAR is situated at the centre of HKIA. Each laser beam consists of 100 range gates and the gate spacing is 100 m, thus having a maximum range of 10 km. It has 3 PPI scans with elevation 0.6, 1.0 and 4.5 degrees respectively. The data are updated every 1-2 minutes. It mainly provides the wind data for lower levels of the atmosphere in clear sky situations.

2.4 *Temporal Resolution*

Since the observation data are updated frequently, the analysis system can provide 3-dimensional analysis as rapid as every 10 minutes. This enables the system to capture small scale, rapidly changing weather phenomena. The temporal resolution chosen is limited by the performance of the computer used Normally, when Doppler radar, TDWR, LIDAR and other remote sensing data are ingested, it would require about 5 to 10 minutes for a commodity computer to complete one single analysis.

3. DATA PREPARATION

All observation data are converted into the NetCDF format for ingestion. For radar and LIDAR data, some more data format conversion steps are required.

Initially, the radar data are arranged in gate-by-gate, polar-azimuthal format. The data were then mapped onto the Cartesian LAPS grids via a remap program. This algorithm will compute the reflectivity and Doppler velocity for each grid by taking the average value of the data points which are lying within that grid volume. As the Doppler weather radar, TDWR and LIDAR have different characteristics, the original LAPS remap algorithm is modified accordingly so that it can process all these kinds of remote sensing data.

Radar data are essential in the analysis of mesoscale and microscale weather systems including microburst. The original setting of the quality check (QC) process in LAPS may filter out the gust wind, as the magnitude of the gust wind may be too large compared with the background wind vectors. To avoid this, the tolerance value in the QC algorithm was set to a large number. Experiments showed that this could retain the gusty winds in the analyses. The only drawback

(a)

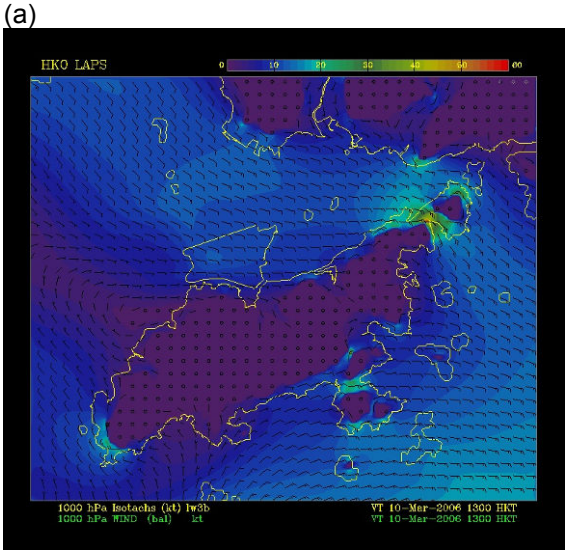

(b)

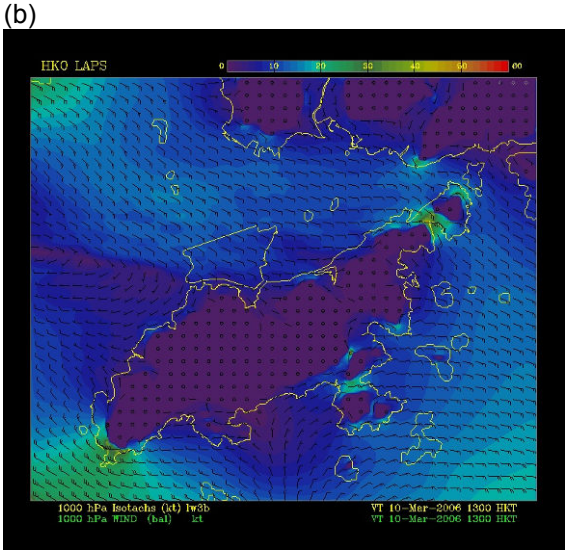

(c)

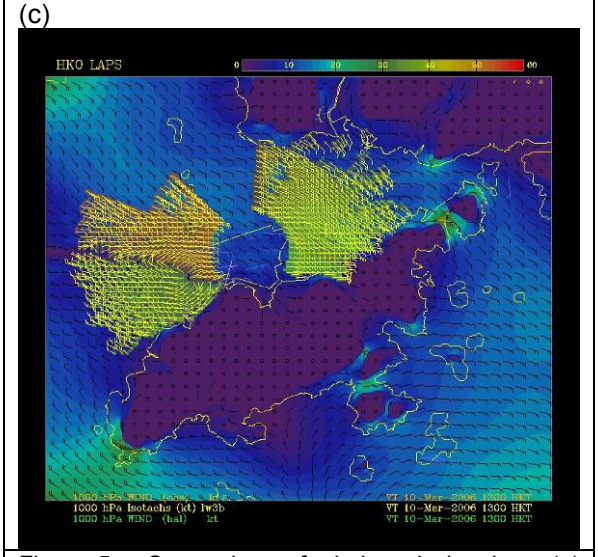

Figure 5 – Comparison of wind analysis where (a) without LIDAR and (b) with LIDAR. (c) is the same as (b) except the LIDAR data (yellow wind barbs) are masked on the image. Background colours represent the magnitude of the wind (see the color legend for the wind speeds).

is that some unwanted wind information, such as folded radial winds which may occur in some radar scans, may also pass the QC and ingested into the system. Thus additional optimization process especially for TDWR data was performed before the remap process to remove contaminated data (Lee and Shun, 1998).

4. CASE STUDIES

4.1 *Sea Breeze (10 Mar 2006)*

Sea breeze is a common phenomenon occurs along the coastal areas. It is developed due to the temperature difference between the water surface and the landmass, when the landmass becomes relatively warmer than the water under solar radiation. This creates a pressure drop over the landmass and thus the air moves from the sea towards the landmass. In this study, the effectiveness of LAPS analysis using LIDAR ingestion is investigated.

Under the influence of a weakened humid maritime airstream, the weather was mild with sunny periods on 10 March 2006. Prevailing wind was generally east in the morning. At about noon (0400 UTC), winds in the northwestern part of the Lantau Island started to change from east to west-southwest under the seabreeze effect. The LAPS analysis results are shown in Fig. 5. Figure 5a is the wind field analysis without LIDAR data ingested while Fig. 5b with LIDAR included. By comparing the two figures, it can be seen that the convergence line is more prominent when LIDAR data were ingested.

Figure 6 shows the time series from 0400 UTC to 0550 UTC, from which the evolution of the seabreeze front can easily be observed. The axis changed from west-east direction to northwest-southeast direction, and the easterly wind in the north of the HKIA weakened, suggesting that the sea breeze was growing stronger. The high temporal resolution of the system enables aviation forecasters to make use of the trend to predict the strength and the location of the convergence zone.

Convergence near the surface is usually associated with increased uplift to aircraft flying through the zone with upward wind. Figure 7a shows the vertical wind analysis, from which it can be seen that the wind in the convergent zone was upward, while the surrounding area was weakly downward in general. A vertical

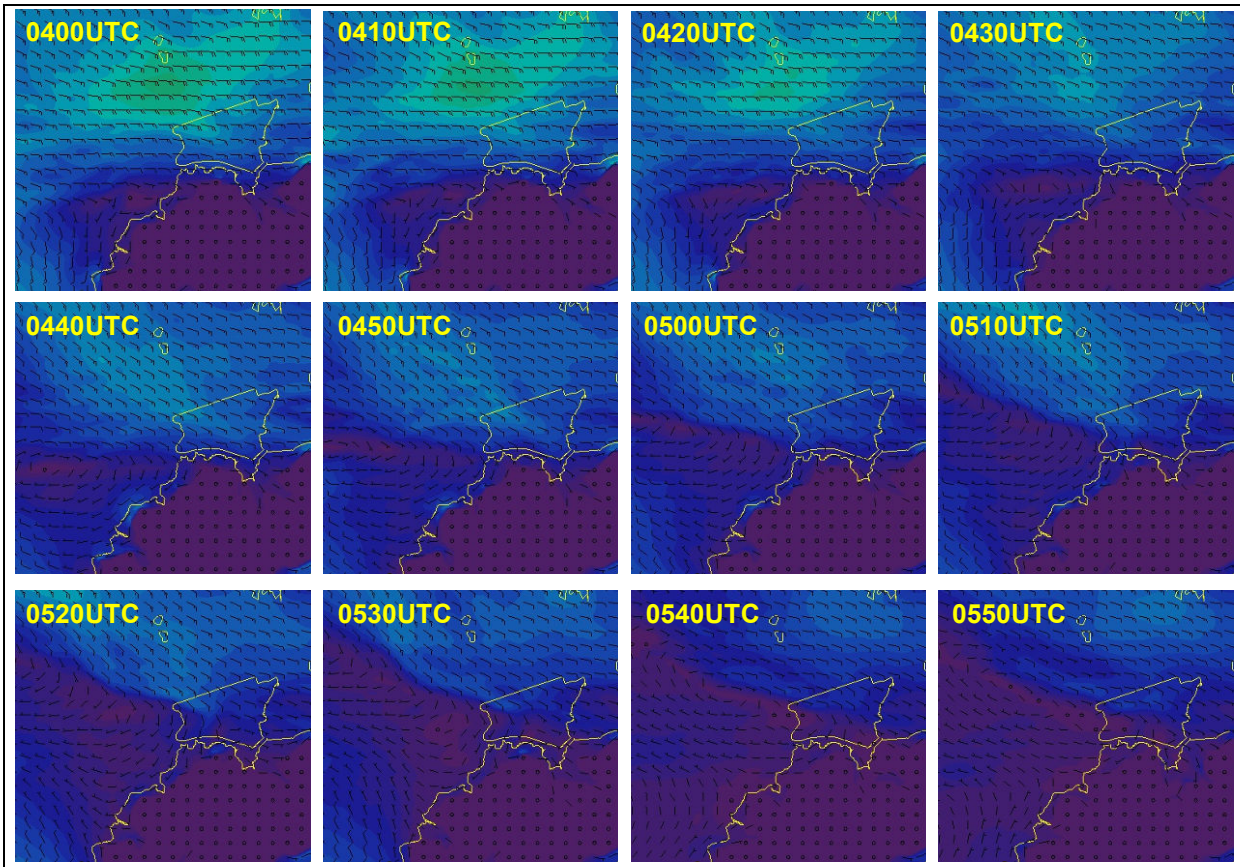

Figure 6 – A time series of analysis. The convergence line, which is the weak wind zone formed under the convergence of the prevalent easterlies with the westerlies due to the seabreeze effect, can be clearly shown.

(a)

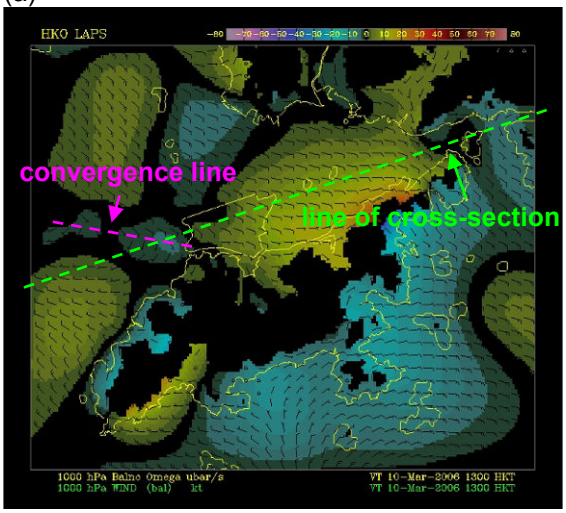

(b)

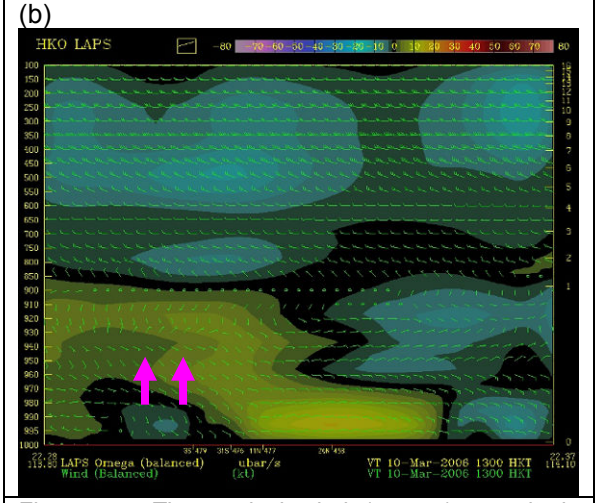

Figure 7 - The vertical wind (omega) magnitude plotted in (a) horizontal domain, and in (b) vertical cross- section along the north runway in HKIA. The yellow color represents positive omega (downward) and the blue color represents negative omega (upward). The green wind barbs in (b) are horizontal winds in each layer.

cross-section along the north runway is also plotted in Fig. 7b. The horizontal wind converged only in the first few layers near the ground surface. This implies that the uplift did not occur in higher levels but only confined to the lower levels up to around 300 m, which was physically reasonable under a stable atmospheric condition.

4.2 *Typhoon Prapiroon (03 Aug 2006)*

Tropical cyclone Prapiroon entered the South China Sea and later intensified into a typhoon on 2 August. It moved west-northwestwards towards the western coast of Guangdong and made landfall at night on 3 August (Fig. 8). The outer rainbands of Prapiroon brought squally heavy showers to Hong Kong and the winds strengthened later on 2 and 3 August.

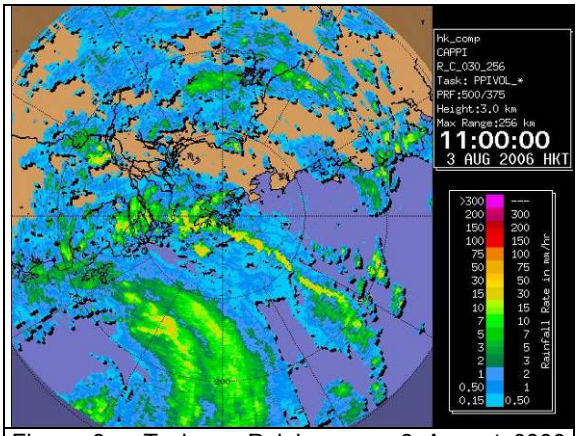

Figure 8 – Typhoon Paipiroon on 3 August 0300 UTC.

At around 11:00 a.m. (0300 UTC) on 3 August, a rainband of Prapiroon swept over the HKIA which brought about 5 mm rainfall within 15-minute over HKIA (Fig. 9). Figure 10a shows the radar reflectivity images captured by the TMS radar. At about 11:48 a.m. (0348 UTC), the rainband had moved away (Fig. 10b) and the rain stopped. At noon (0400 UTC), small convective clouds developed and scattered around HKIA (Fig. 10c), bringing only trace amount of rainfall to HKIA.

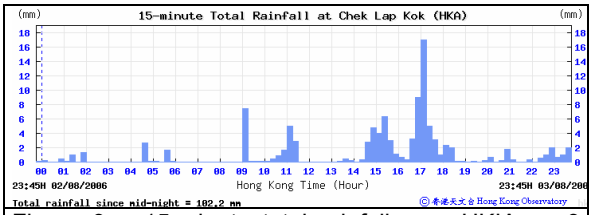

Figure 9 – 15-minute total rainfall over HKIA on 3 August.

Analysis of the above time period was conducted (Fig. 11). Since there were heavy rains over HKIA on 0300 UTC, the infrared laser beams emitted by the LIDAR were absorbed by the raindrops and as a result, there was no return signals from the LIDAR. Nonetheless, the TDWR accomplished that during that period and provided information on the radial velocity of the raindrops (Fig. 11a). In contrast, at 0348 UTC, as there was no precipitation, none signal emitted by the TDWR returned. Fortunately, the presence of LIDAR became the major contributor on the velocity data as shown in Fig. 11b. At 0400 UTC, with the presence of scattered light rain, both LIDAR and radar operated effectively to provide velocity data simultaneously (Fig. 11c). LIDAR and radar data in this case are complementary to each other to provide continuous information for wind analysis.

(a)

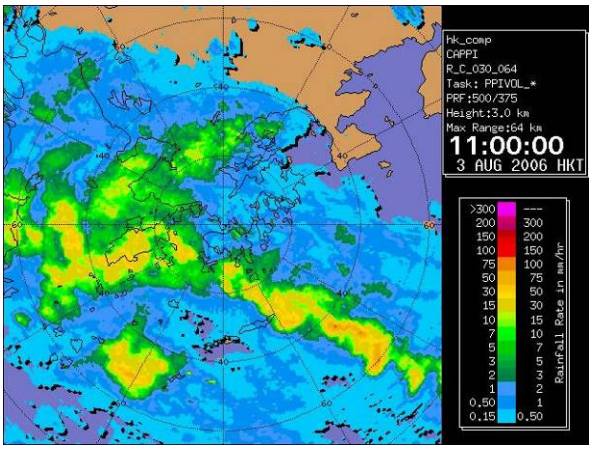

(b)

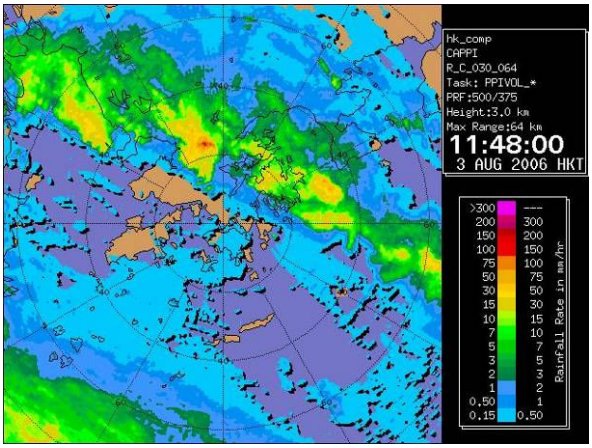

(c)

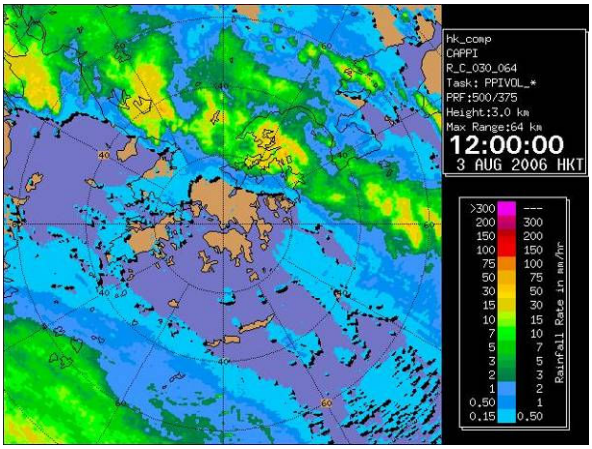

Figure 10 – 64-km range radar reflectivity over Hong Kong for (a) 0300 UTC, (b) 0348 UTC and (c) 0400 UTC.

(a)

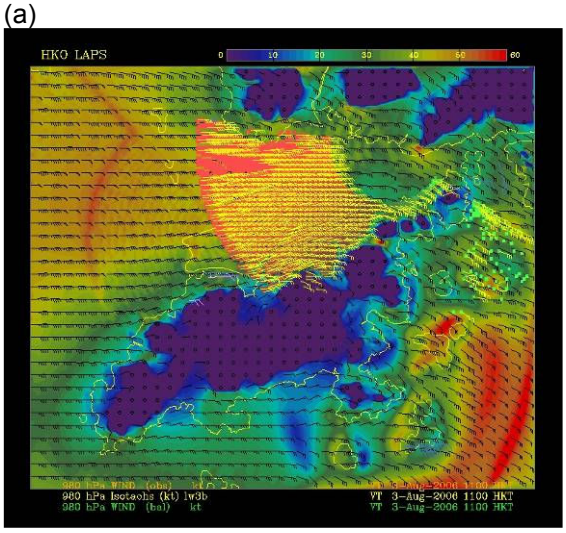

(b)

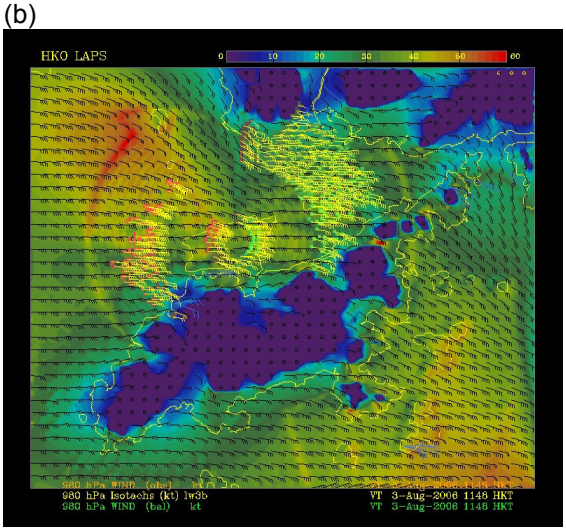

(c)

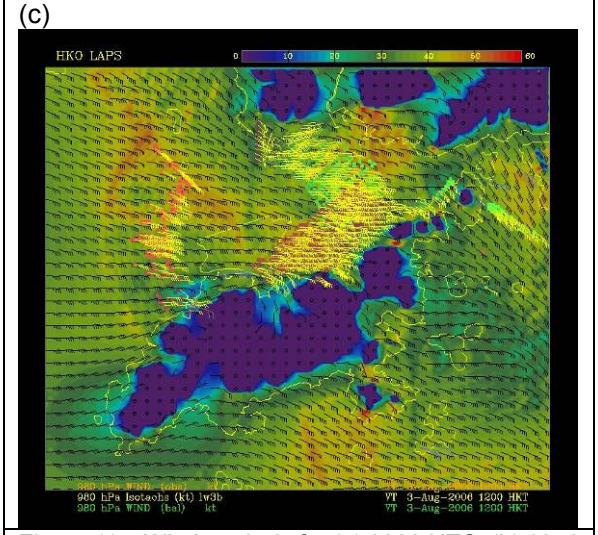

Figure 11 – Wind analysis for (a) 0300 UTC, (b) 0348 UTC and (c) 0400 UTC. Radar and LIDAR data (both in yellow wind barbs) are masked on the image.

4.3 *Microburst (08 Jun 2007)*

A trough of low pressure over southern China was moving slowly towards the coast early June 2007 and brought a week of unsettled weather to Hong Kong. In the morning on 8 June, squally thunderstorms affected the HKIA (Fig. 12). At about 9:45 a.m. (0145 UTC), a helicopter parking on the apron was toppled under the wind gust brought by the downburst.

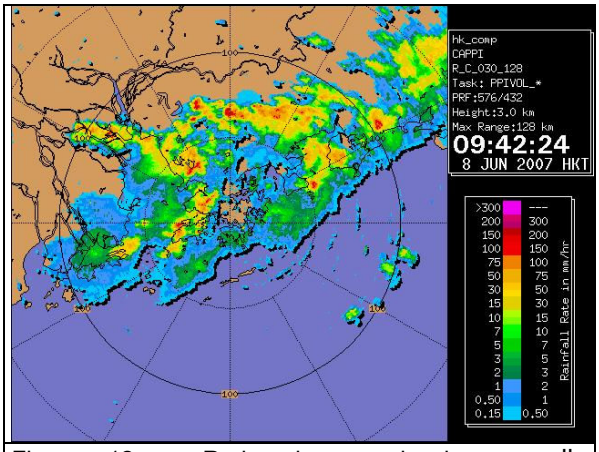

Figure 12 – Radar image showing squally thunderstorms approaching HKIA on 8 June.

To understand what might have happened during the incident, a number of LAPS analyses were done for 0145 UTC and the times around. Figure 13 shows the surface wind distribution over the HKIA analyzed by LAPS. It can be seen that the winds near the GFS apron were strongest over 50 knots. Analysis of the evolution of the storm as shown on the radar images suggested that the gusty winds were brought by a microburst.

In order to further confirm the existence of the microburst, a storm motion analysis was performed. The average wind vector over the HKIA area was calculated and each wind vectors in the area was then subtracted by the average wind vector. This procedure was performed on different pressure levels and the result on the lowest level was shown in Fig. 14. As can be seen, an anti-cyclonic diverging field was detected in low level layers, with a divergence of about 0.4 s^{-1}. This is comparable to the divergence value in radial direction calculated from solely TDWR observations, which is 0.18 s^{-1}. According to Fujita (1981), this value of divergence with a lifetime of 2 to 10 minutes could be a misohigh system with downburst associated with thunderstorms. Our analysis supports the conjecture that the strong gusty winds were originated from a microburst.

(a)

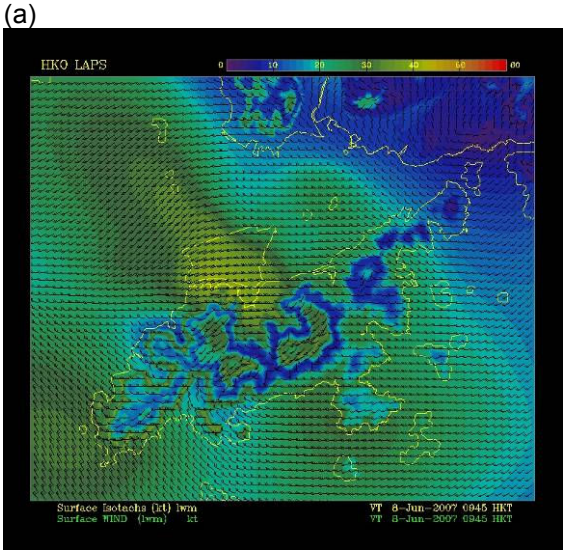

(b)

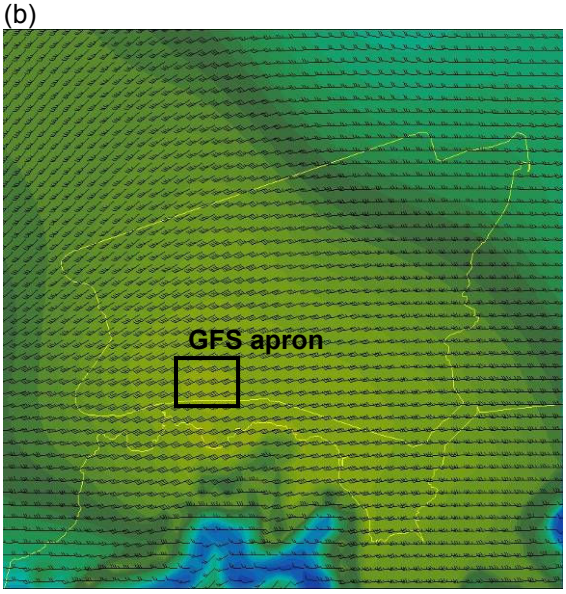

Figure 13 – Surface wind analysis plotted in (a) whole horizontal domain, and (b) zoomed into HKIA, which shows that the winds are strongest near the southwest apron.

5. CONCLUSIONS

A high resolution meteorological data analysis system has been developed for aviation forecasters to grasp the atmospheric conditions of the rapidly changing weather over HKIA and its vicinity. With the high resolution background and observation data ingested, the system can help monitor the mesoscale to microscale weather systems, including sea breeze and microburst. As LIDAR and weather radar data are complementary to each other, the system can provide high quality analyses under nearly all-weather conditions. This is especially important in situations of unsettled weather.

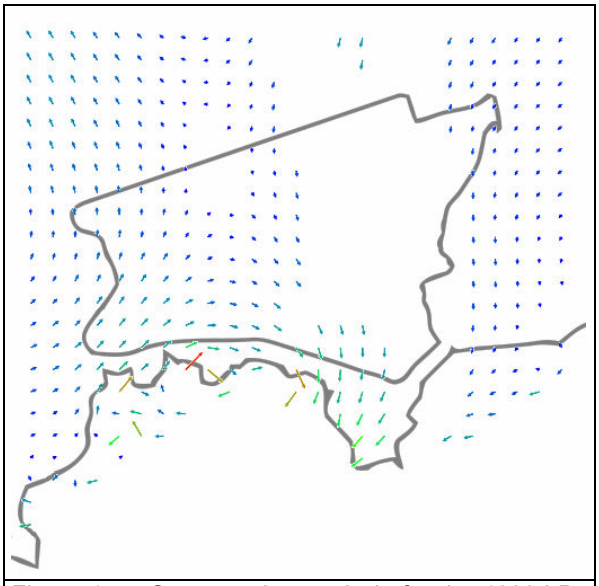

Figure 14 – Storm motion analysis for the 1000-hPa layer. An anti-cyclonic divergence flow associated with the microburst can be found, with its center located just to the southwest of HKIA.

A number of developments could be conducted to further enhance the capabilities of the system. Take the microburst case as an example. Although the horizontal wind is consistent with the observation data, the vertical wind, especially the downdraft, is weaker than expected. Consequently, further works have to be done on the vertical wind analysis in order to obtain a more comprehensive three-dimensional picture of the atmosphere around HKIA.

Last but not the least, the focus of the present work has been put on the archived case studies. The next step is to run the system in real-time to collect more real-time cases. We might consider running the system every 10 minutes, or even every 5-6 minutes with the advance of computation power.

6. ACKNOWLEDGEMENT

The authors would like to thank Mr. M.W. Yau for his early development work of the system.

7. REFERENCES

Albers S., 1995: The LAPS wind analysis. *Weather and Forecasting*, **10**, 342-352.

Albers S., J. McGinley, D. Birkenheuer, and J. Smart, 1996: The Local Analysis and Prediction System (LAPS): Analyses of clouds, precipitation, and temperature. *Weather and Forecasting*, **11**, 273-287.

Fujita T.T., 1981: Tornadoes and downbursts in the context of generalized planetary scales. *J. Atmos. Sci.*, **38**, 1511-1534.

Fujita T.T., 1985: The Downburst- Microburst and Macroburst, Satellite and Mesometeorology Research Project (SMRP) Research Paper 210, Dept. of Geophysical Sciences, Univ. of Chicago, 122 pages.

Lee O.S.M. and Shun C.M., 1998: Optimization of the Terminal Doppler Weather Radar for the Hong Kong International Airport. *Proceedings of International Symposium on Electronic in the Air Transport Industry 98'*, Hong Kong, China, November 1998.

McGinley, J.A. and J.R. Smart, 2001: On providing a cloud-balanced initial condition for diabatic initialization. *Preprints, 18th Conf. on Weather Analysis and Forecasting*, Amer. Meteor. Soc.